RSC Advances

PAPER

View Article Online
View Journal | View Issue

Cite this: *RSC Adv.*, 2025, **15**, 35099

Capillary-based pH-responsive nano-enzymatic SERS sensors for the diagnosis of *Helicobacter pylori*

Yangfan Zhou, †[b] Caili Bi,†[b] Tengfei Pang,†[ab] Yanwen Zhuang,[b] Yayun Qian [b] and Fengsong Chen *[a]

The accurate and sensitive detection of urease in saliva is the key to detecting *Helicobacter pylori* (*H. pylori*) infection. In this study, we developed a pH-responsive nano-enzymatic surface-enhanced Raman scattering (SERS) sensor for the indirect detection of urease concentration, with assembled nano-enzymatic gold core-palladium shell nanorods (Au@Pd NRs) on the inner wall of the capillary. The nano-enzymatic nanorods could catalyze the oxidation of 3,3′,5,5′-tetramethylbenzidine (TMB) by hydrogen peroxide (H_2O_2) to produce oxidized TMB (ox-TMB) with a strong SERS signal. When urease is present in the liquid taken up by the capillary, it specifically hydrolyzes urea, which increases the pH of the solution, inhibits the catalytic activity of the nano-enzyme and reduces the production of ox-TMB, leading to a decrease in the SERS signal and thus enabling the indirect detection of the concentration of urease. The sensor demonstrates excellent analytical performance with a low limit of detection (LOD) of 6.09 U L^{-1}, and the detection process could be completed within 15 min. For real saliva samples, the results showed significant correlation with the urease test kit, enabling rapid and accurate detection of urease concentration in saliva samples from healthy individuals and *H. pylori* patients. Receiver operating characteristic (ROC) curves were used to evaluate the diagnostic efficacy of the sensor for detecting *H. pylori*, and the analysis showed that the area under the ROC curve (AUC) was 0.959, which is promising for application in clinical diagnosis.

Received 14th July 2025
Accepted 10th September 2025

DOI: 10.1039/d5ra05046d

rsc.li/rsc-advances

1. Introduction

Helicobacter pylori (*H. pylori*) is a spiral, slightly anaerobic, Gram-negative bacillus capable of surviving in a strongly acidic environment, and its unique spiral morphology and adhesive properties allow it to colonize the gastric mucosa for long periods of time in a strongly acidic environment.[1,2] Clinical outcomes due to *H. pylori* infection show significant heterogeneity:[3] About 70% of *H. pylori*-infected patients are asymptomatic carriers, 10–15% may develop peptic ulcers, and 1% eventually progress to gastric cancer.[4–6] Currently, there are mainly invasive and non-invasive tests for the determination of *H. pylori*. Invasive tests include isolation and culture of *H. pylori*, smear examination, rapid urease test and drug sensitivity test.[7,8] The results of isotopic analysis were compared with the findings of the histopathological evaluation of gastric biopsies, which is the gold standard to detect *H. pylori* infection.[9] Non-invasive tests include the ^{13}C-urea and ^{14}C-urea breath tests, as well as the detection of *H. pylori* antigens in feces and *H. pylori* antibodies in serum by immunologic methods.[10] All of the above tests require specialized physicians, do not allow for large-scale screening, and do not provide rapid results. Therefore, it is necessary to develop a simple, convenient, highly sensitive test for *H. pylori* that can be performed on a large scale. Research has revealed that individuals infected with *H. pylori* not only exhibit high levels of urease activity in their stomachs but also have significantly higher urease concentrations in their saliva compared to uninfected individuals.[11–13] Therefore, measuring urease concentration in saliva has emerged as a potential non-invasive method for diagnosing *H. pylori* infection, with a principle similar to that of the urea breath test.

Surface-enhanced Raman scattering (SERS) is a vibrational spectroscopy technique capable of responding to the characteristic structure of a molecule, which utilizes unique molecular vibrational fingerprint information to identify and quantify analytes.[14–16] When molecules or ions are adsorbed onto the rough surface of metal nanomaterials, the originally weak Raman scattering signals are significantly enhanced, which greatly improves the detection sensitivity of molecular "fingerprinting" information, and realizes the non-invasive, rapid, and accurate detection of molecules in an aqueous environment.[17–19]

[a]*Department of Gastroenterology, Haimen People's Hospital, Nantong, 226000, People's Republic of China. E-mail: cfs@sina.com*

[b]*Institute of Translational Medicine, Medical College, Yangzhou University, Jiangsu Key Laboratory of Integrated Traditional Chinese and Western Medicine for Prevention and Treatment of Senile Diseases, Yangzhou, 225001, P. R. China*

† Co-first authors.

In recent years, nano-enzymatic materials with certain enzyme mimetic activities have gradually emerged, and they have the advantages of high stability, adjustable catalytic activity, specificity, versatility, and ease of preparation,[20] which have demonstrated extraordinary application potential in the fields of basic research and clinical testing.[21] For example, when nanoenzymes catalyze the oxidation of 3,3′,5,5′-tetramethylbenzidine (TMB) by hydrogen peroxide (H_2O_2), they can produce oxidized TMB (ox-TMB) in a blue color with a higher intensity of SERS signals, a property that provides an innovative idea for the detection of highly sensitive targets.[22,23] Therefore, combining SERS and the peroxidase-like (POD-like) activity of nanoenzymatic materials to construct a nano-enzymatic SERS sensor can effectively improve detection efficiency and sensitivity, and provide a promising novel method for the detection of highly sensitive targets.

Existing SERS substrates are mainly prepared on planar solid materials (such as silicon and glass wafers) using lithography and self-assembly techniques.[24] These planar substrates are detected by immersion in a sample solution or by dropping the sample solution onto the surface after drying.[25] However, the efficiency of sample collection has a great influence on SERS test results in practical applications.[26] Particularly, when facing some irregular planar extraction samples, the planar substrate is unable to carry out efficient sampling work, and the sample molecules are exposed to the air during the detection process, which is more likely to be contaminated by the external environment.[27,28] Therefore, planar substrates have some limitations for trace analysis and on-site rapid detection in various fields, especially in the field of biomedical testing. In recent years, capillary-based SERS sensors have attracted widespread attention due to their unique properties and advantages. The capillary tube can utilize its own capillary force to draw liquid samples into the capillary tube to obtain their SERS spectra, which is more suitable for liquid-phase detection in practical applications.[29,30] Capillary SERS sensors can protect the sample to be measured from the detection environment after drawing it, which can effectively improve signal repeatability. In addition, it is expected to be an ideal platform for on-site microanalysis due to its advantages of low sample consumption, high optical transmittance, low cost, and ease of fabrication.[31]

In this study, we developed a pH-responsive nano-enzymatic SERS sensor that combines the POD-like activity of nanoenzymatic material with SERS technology to achieve the rapid, sensitive, and accurate detection of urease concentration in solution. The flow of this study is shown in Fig. 1. First, we immersed the aminated capillary into a gold core-palladium shell nanorods (Au@Pd NRs) solution for self-assembly to obtain the nano-enzymatic SERS sensor (Fig. 1(A)), which has good POD-like activity and SERS enhancement ability. Urea was then added to the test solution to fully react, and then a mixed solution of TMB, H_2O_2, and PBS was added to the reaction solution. The nano-enzymatic SERS sensor was placed vertically into the mixed solution to react. If there was no urease in the solution to be tested, due to the existence of a suitable reaction

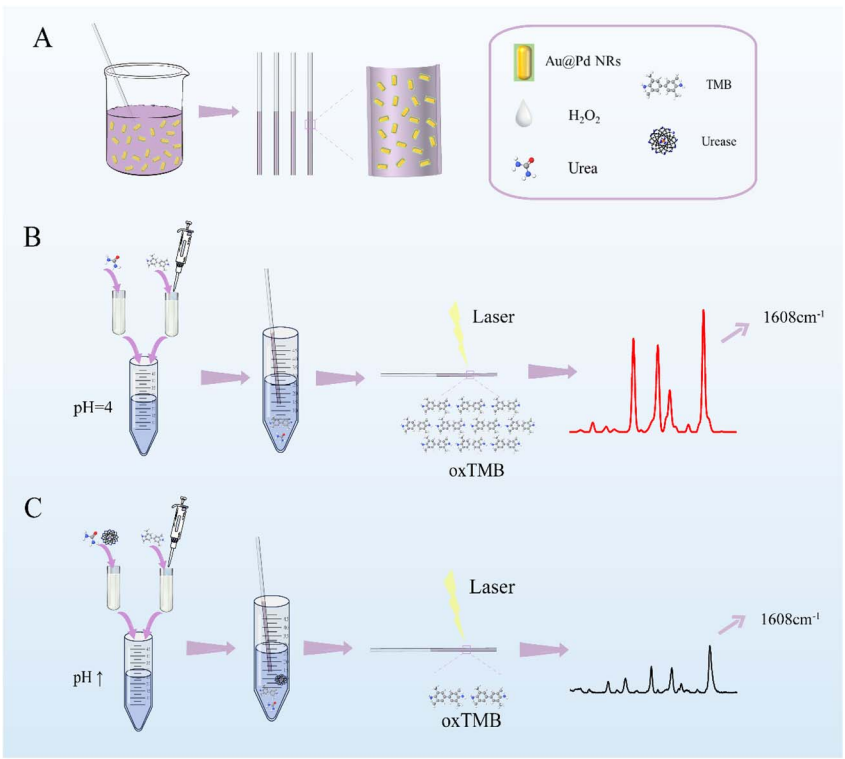

Fig. 1 (A) The preparation process of the nanozyme SERS sensor. (B) The detection process of the nanozyme SERS sensor for samples without urease. (C) The detection process of the nanozyme SERS sensor for samples containing urease.

environment, Au@Pd NRs would catalyze the oxidation of TMB by H_2O_2 to generate oxidized TMB with higher SERS signals (ox-TMB) (Fig. 1(B)). Urease has the specific ability to hydrolyze urea to produce ammonia. When urease is present in the solution to be tested, the specific hydrolysis of urea to produce NH_3 and H_2O increases the pH of the solution and reduces the catalytic activity of the nano-enzymatic Au@Pd NRs, leading to a lower yield of ox-TMB and a weakening of the SERS signals (Fig. 1(C)) based on the characteristic peak of ox-TMB at 1608 cm^{-1} intensity, thus indirectly detecting the concentration of urease. The sensor was used for the clinical testing of actual saliva samples. Saliva samples from healthy individuals and Hp patients were centrifuged and processed for SERS testing according to the process above, realizing the rapid, sensitive, and accurate detection of urease concentration in clinical samples, providing a new technological option for point-of-care testing (POCT) of *Helicobacter pylori* infection.

2. Experimental section

2.1 Materials and reagents

Palladium chloride ($PdCl_2$), chloroauric acid tetrahydrate ($HAuCl_4$), sodium borohydride ($NaBH_4$), ascorbic acid (AA), cetyltrimethylammonium bromide (CTAB), potassium iodide (KI_3), 3,3′,5,5′-tetramethylbenzidine (TMB), hydrochloric acid (HCl, 37 wt%), hydrogen peroxide (H_2O_2), sodium oleate (NaOL), anhydrous ethanol, phosphate buffered saline (PBS), aminopropyltriethoxysilane (APTES) and polyvinyl pyrrolidone (PVP) were purchased from Sinopharm Chemical Reagent Co. Urease and urea were purchased from Beijing Solarbio Science & Technology Co. All chemicals were used without further purification. The capillary tubes used in the experimental setup were purchased from Beijing Jitian Biotechnology Co. All solutions were prepared in deionized water (18.2 MΩ cm) to ensure that precise experimental conditions were maintained.

2.2 Equipment

Transmission electron microscope (TEM) images were obtained using a Tecnai 12 transmission electron microscope, while scanning electron microscope (SEM) images were acquired with an S-4800 II field-emitting scanning electron microscope. Elemental mapping images were captured with a Tecnai G2 F30 field-emission transmission electron microscope, and SERS mapping images were obtained with a DXRxi micro-Raman imaging spectrometer. Ultraviolet-visible-near-infrared (UV-vis-NIR) absorption spectra were obtained using a UNICO 2100 PC UV-visible spectrophotometer, and SERS spectra were obtained using an inVia Raman spectrometer (Renishaw, UK). The kinetic parameters of the enzymatic reaction were determined using a BioTek Epoch™ Microplate Spectrophotometer (BioTek, USA), and the Michaelis–Menten equation was used to fit the experimental data. A double inverse Lineweaver–Burk plot was made to analyze the kinetic characteristics of the enzymatic reaction.

2.3 Preparation of Au@Pd NRs

Gold nanorods were synthesized according to the seed-mediated scheme described previously in the literature with some slight optimizations.[32] The gold seed solution was first prepared. $HAuCl_4$ (0.5 mM, 5 mL) solution was added to the CTAB solution (0.2 mM, 10 mL) with vigorous stirring, and then $NaBH_4$ (0.01 mM, 1.2 mL) solution was added quickly with continuous stirring for 1 min. The gold seed solution was allowed to stand at 30 °C for 30 min. The growth solution for the seeds was then prepared. To 200 mL of ultrapure water, 4 g of CTAC and 0.8 g of NaOL were added to fully dissolve, and $AgNO_3$ (4 mM, 14 mL) solution and $HAuCl_4$ (100 mM, 200 mL) solution were added sequentially to the above solutions, and stirring was continued for 2 h at 30 °C. Subsequently, HCl (37 wt%, 1.2 mL) was added, and AA (64 mM, 1.4 mL) was added rapidly after vigorous stirring for 15 min. Then, 2 mL of the gold seed solution was added after continuous vigorous stirring for 30 s, and stirring was continued for 15 min. The solution was then allowed to stand at a temperature of 30 °C for 12 h. Finally, the solution was centrifuged at 8000 rpm for 15 min and washed three times with ultrapure water to prepare the obtained Au NPs solution. The next step was to synthesize Au@Pd NRs by the seed growth method. A 0.01 M solution of $PdCl_2$ was prepared by adding $PdCl_2$ powder to HCl (50 mL, 0.02 M) to dissolve it fully, then it was placed in a 60 °C water bath. Au NRs (0.5 mL), $PdCl_2$ (0.2 mL, 0.01 M), and KI_3 (0.15 mL, 0.01 M) were then sequentially added to the CTAB (9.15 mL, 0.01 M) solution with vigorous stirring. After rapidly injecting AA (0.08 mL, 0.1 M) into the mixed solution, it was placed in a water bath at 50 °C for 2 h. Finally, it was centrifuged at 8500 rpm for 6 min and washed three times with ultrapure water to obtain the Au@Pd NRs, which were then dispersed in ultrapure water.

2.4 Amination of capillaries

The capillary was ultrasonicated with ultrapure water twice, for 20 min each time, and then twice with anhydrous ethanol, for 20 min each time. Subsequently, it was ultrasonicated with anhydrous ethanol twice. After ultrasonication, the capillary was dried and placed in a 10% APTES ethanol solution and heated in an oven at 85 °C for 4 h. Next, the capillary was cleaned by ultrasonication with anhydrous ethanol to remove APTES residues. This ultrasonic cleaning process was carried out twice, with each session lasting for 10 min. During the ultrasonic cleaning, the capillary was continuously observed to check for the presence of any white hanging material on the inner wall. The cleaning was continued until the inner wall of the capillary became transparent and free of impurities. Finally, the capillary was dried to obtain the aminated capillary.

2.5 Self-assembly of capillaries

The Au@Pd NRs were cleaned to remove the residual synthetic reagents, then they were dispersed into a 1% PVP solution, sonicated for 20 min, and left to stand for 30 min. Centrifugation was then used to remove the remaining PVP. The Au@Pd NRs were dispersed into 0.2 mL of anhydrous ethanol to prepare

a concentrate of PVP-wrapped Au@Pd NRs, which both prevents the agglomeration of Au@Pd NRs and regulates the surface charge to increase the interaction with capillaries. After sufficient sonication and dispersion, a certain amount of the concentrate was drawn into an aminocarbonate capillary tube and left to stand for 30 min. Subsequently, a pipette bulb was employed to blow out the concentrate, and the Au@Pd NRs on the outer wall of the capillary were wiped off. The capillary was then washed three times by sucking anhydrous ethanol to wash the inner wall, ensuring the removal of unassembled nanoparticles. After that, the capillary was dried for later use, and then the nano-enzymatic SERS sensors were obtained.

2.6 SERS measurement

During the detection process, the solution to be tested was mixed and reacted with urea (1 M), then H_2O_2 (0.5 M), TMB (0.8 mM), and PBS buffer were added to the mixed solution. After inserting the nano-enzymatic SERS sensor vertically into the mixed solution and reacting, the capillary was subjected to Raman detection, and SERS spectra were obtained. The Raman spectrometer was used with a 50× objective lens, a laser wavelength of 785 nm, an exposure time of 10 s, and a power of 5 mW. To ensure the credibility and validity of the results, for each sample to be collected, three points at different positions on the capillary were selected, and the average value was calculated.

3. Results and discussion

3.1 Characterization of Au@Pd NRs

We conducted a comprehensive characterization of the prepared Au@Pd NRs, focusing on their shape and structure, using high-resolution transmission electron microscopy (HRTEM). HRTEM images of Au@Pd NRs are shown in Fig. 2(A). The Au@Pd NRs exhibited a square-nanorod morphology, with a length of 95 nm and a width of 40 nm. They possess a uniform topographic size and an aspect ratio of approximately 2.4 : 1. To obtain information related to Au@Pd NRs, we acquired the XRD patterns (Fig. S1), and in the 2θ = 30–50° range, the patterns of Au@Pd NRs showed characteristic peaks of Au with a face-centered-cubic (FCC) structure (2θ = 38.2 and 44.4°) and characteristic peaks of Pd (2θ = 40.1 and 46.7°), corresponding to the {111} and {200} planes, respectively. The data indicate that Au@Pd NRs are composed of FCC crystals. To further investigate the structure of Au@Pd NRs, we obtained lattice images (Fig. 2(B)) and SAED images (Fig. 2(C)) of Au@Pd NRs. The lattice image shows that the lattice stripes with a pitch of 0.225 nm correspond to the {111} planes of the FCC Pd, and the SAED image shows that the Au@Pd NRs are polycrystalline in structure. We also conducted energy-dispersive X-ray (EDX) spectroscopy and elemental mapping. As shown in Fig. 2(D), the Au@Pd NRs exhibit distinct core–shell structures, comprising dense gold nanorods (Au NRs) as the inner core and a palladium (Pd) shell layer tightly adhered to the exterior of the gold

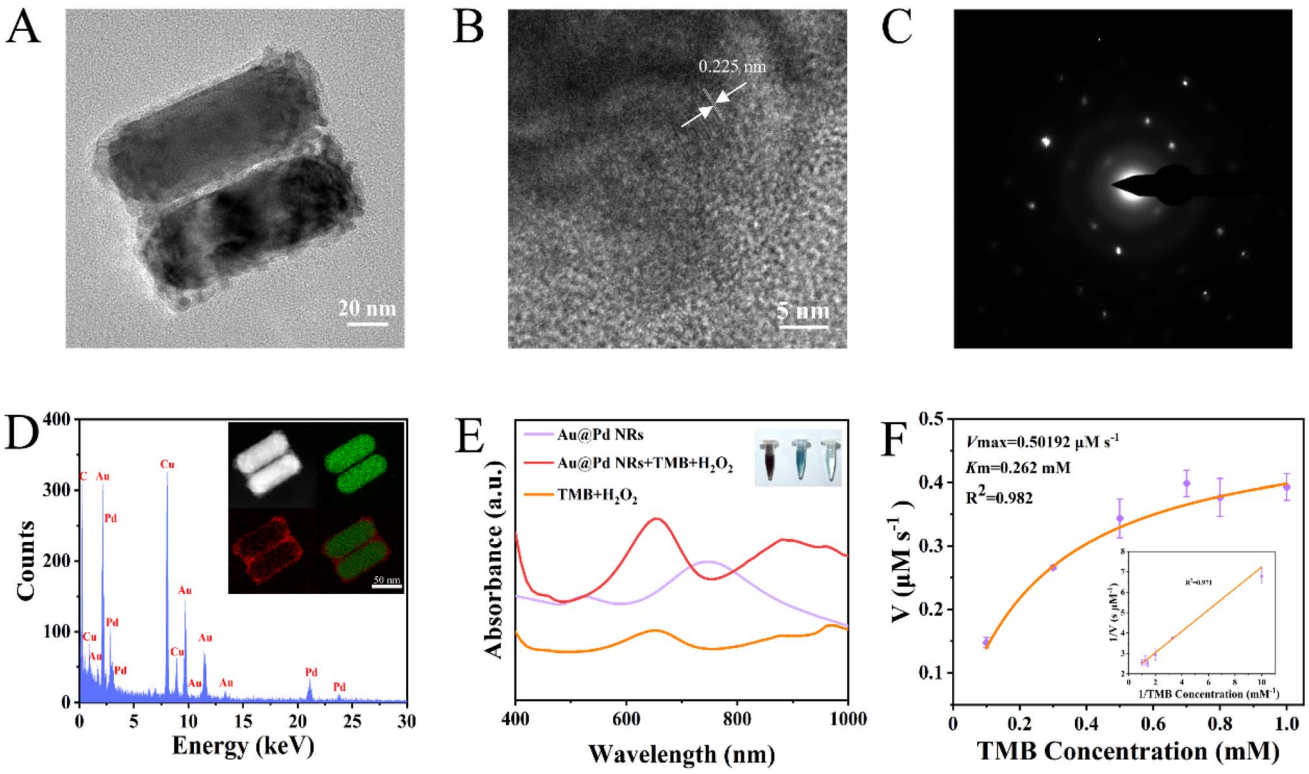

Fig. 2 (A) HRTEM image of Au@Pd NRs. (B) Lattice image of Au@Pd NRs. (C) SAED image of Au@Pd NRs. (D) EDX spectra and elemental mapping of Au@Pd NRs. (E) UV-vis absorption spectra and solution color changes catalyzed by Au@Pd NRs. (F) Michaelis–Menten curve and the corresponding double inverse curve for nano-enzymatic Au@Pd NRs.

nanorods. The EDX images also reveal that the constituent elements of the Au@Pd NRs are Au and Pd, while the elemental Cu is sourced from the supporting Cu network for the Au@Pd NRs. The UV-vis absorption spectra (Fig. 2(E)) show that the Au@Pd NRs solution exhibited a grayish-purple color, and the position of its UV absorption peak was at 748 nm. The solution turned blue only when the Au@Pd NRs were mixed with H_2O_2 and TMB, and an obvious absorption peak was observed at 652 nm, indicating that the Au@Pd NRs possess good POD-like activity. In addition, we conducted steady-state kinetic analysis to investigate the catalytic activity of Au@Pd NRs. As shown in Fig. 2(F), we obtained a typical Michaelis–Menten curve and a double inverse curve. The catalytic parameters (K_m and V_{max}) were calculated using Michaelis–Menten fitting and the double-reciprocal method based on the Lineweaver–Burk equation: $1/v = (K_m/V_{max})(1/[S] + 1/K_m)$. Here, v represents the initial reaction rate, V_{max} is the maximum reaction rate, K_m is the Michaelis–Menten constant, and [S] corresponds to the concentration of the substrate.[33] Then, we calculated $V_{max} = 0.50192$ μM s^{-1} and $K_m = 0.262$ mM. A smaller K_m value indicates a higher affinity of the enzyme for the substrate molecule. V_{max} is a measure of the catalytic activity of the enzyme, and the results demonstrated that Au@Pd NRs exhibited superior catalytic activity.

3.2 Characterization of nano-enzymatic SERS sensors

We prepared capillaries with Au@Pd NRs assembled on the inner wall as high-performance SERS active substrates. Fig. 3(A) presents the physical appearance of the capillary containing Au@Pd NRs. Compared with the blank capillary, it clearly shows the presence of the attached nanomaterials. The SEM image of the nano-enzymatic SERS sensor is displayed in Fig. 3(B). Many clean Au@Pd NRs were dispersed and were found to be structurally intact and morphologically homogeneous, thus demonstrating good dispersion. To investigate the homogeneity of the nano-enzymatic SERS sensor, we performed SERS Mapping. Fig. 3(C) shows a large green color, which indicates that the signals of the sensor have good homogeneity. To evaluate the SERS enhancement effect of the Au@Pd NRs analytical platform, we using DTNB as the signaling molecule. We measured the SERS profile of the DTNB-labeled nano-enzymatic SERS sensor (DTNB-labeled Au@Pd NRs) compared with the Raman spectrum of pure DTNB (Fig. 3(D)). The DTNB-labeled Au@Pd NRs exhibited a significant enhancement of the characteristic SERS peaks at 1332 cm^{-1}, indicating good SERS activity. The enhancement factor (EF) value was calculated using the following formula:

$$EF = (I_{SERS}/C_{SERS})/(I_{RS}/C_{RS}).$$

Here, I_{SERS} and I_{RS} respectively represent the signal intensities of DTNB-labeled Au@Pd NRs and pure DTNB. C_{SERS} and C_{RS} denote the DTNB concentrations, with C_{SERS} being 10^{-8} M for the DTNB-labeled Au@Pd NRs and C_{RS} being 10^{-2} M for pure DTNB. The calculated EF was 2.087×10^8, indicating that Au@Pd NRs are an excellent substrate for SERS. In addition, the prepared nano-enzymatic SERS sensors were used to test their stability by measuring the SERS intensities after being stored at

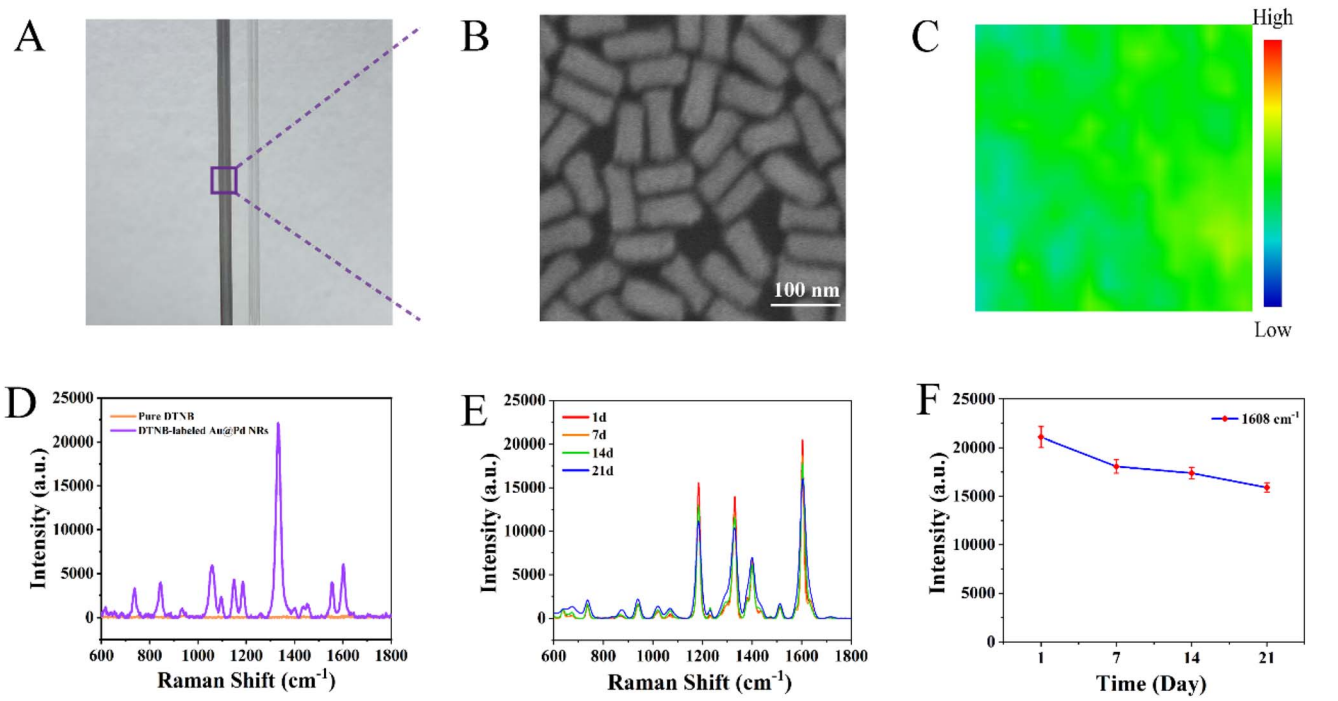

Fig. 3 (A) Images of the assembled Au@Pd NRs capillary and blank capillary. (B) Localized SEM image. (C) SERS mapping image of the nano-enzymatic SERS sensor. (D) SERS spectra of pure DTNB and DTNB-labeled Au@Pd NRs. (E) SERS spectra of nano-enzymatic SERS sensors stored at room temperature for different times. (F) SERS intensity folding maps at 1608 cm^{-1} corresponding to the characteristic peak.

room temperature for different periods (1 d, 7 d, 14 d, and 21 d); the results are shown in Fig. 3(E) and (F). Although the intensity of the characteristic peak at 1608 cm^{-1} weakened, the morphology of the SERS spectra remained essentially unchanged. This result verifies the stability of the nano-enzymatic SERS sensor.

3.3 Feasibility verification of urease detection

To verify the feasibility of the nano-enzymatic SERS sensor for urease detection, we used the sensor to detect a blank solution and a 30 U per L urease solution, and the measured SERS spectra are shown in Fig. 4(A). Compared with the blank solution without urease, when the 30 U per L urease solution was detected, the reaction of urease with urea increased the solution pH, which inhibited the activity of the nano-enzymes and led to a significant decrease in the SERS intensity at the characteristic peak at 1608 cm^{-1} (Fig. 4(B)), demonstrating the feasibility of this method in detecting urease. The specificity of the sensor is also a key factor affecting the feasibility of urease measurement. We introduced amylase, lysozyme, and alkaline phosphatase (AKP) as interferents for the SERS measurement. We used sensors to detect the same concentration of urease, amylase, lysozyme, and alkaline phosphatase (AKP); the resulting SERS spectra are shown in Fig. 4(C) and (D). Urea can only be specifically hydrolyzed by urease, producing water and ammonia gas, which increases the pH of the solution, and the SERS signal intensity of the characteristic peak at 1608 cm^{-1} decreases. Other interfering substances cannot hydrolyze urea, so the pH of the solution does not change, and the SERS signal intensity remains unchanged.

3.4 Optimization of experimental conditions

To achieve the best experimental results, we systematically optimized several key experimental parameters, including detection time, detection temperature, and buffer pH. Detection time is a crucial parameter for the assay, and the performance of the sensor can be further enhanced by optimizing the detection time. As shown in Fig. 5(A), when urease was present in the mixed solution, the intensity of the characteristic peak located at 1608 cm^{-1} decreased over time, and the signal intensity stabilized at approximately 15 min. Therefore, we determined 15 min to be the optimal detection time. Subsequently, we investigated the effect of the detection temperature of the sensor on its POD-like activity, as shown in Fig. 5(B), the SERS signal intensity was enhanced with increasing temperature, and the SERS intensity of the characteristic peak located at 1608 cm^{-1} reached a maximum at a temperature of 30 °C, and then began to weaken, suggesting that the catalytic activity of Au@Pd NRs was strongest at 30 °C. The pH of the buffer is a key

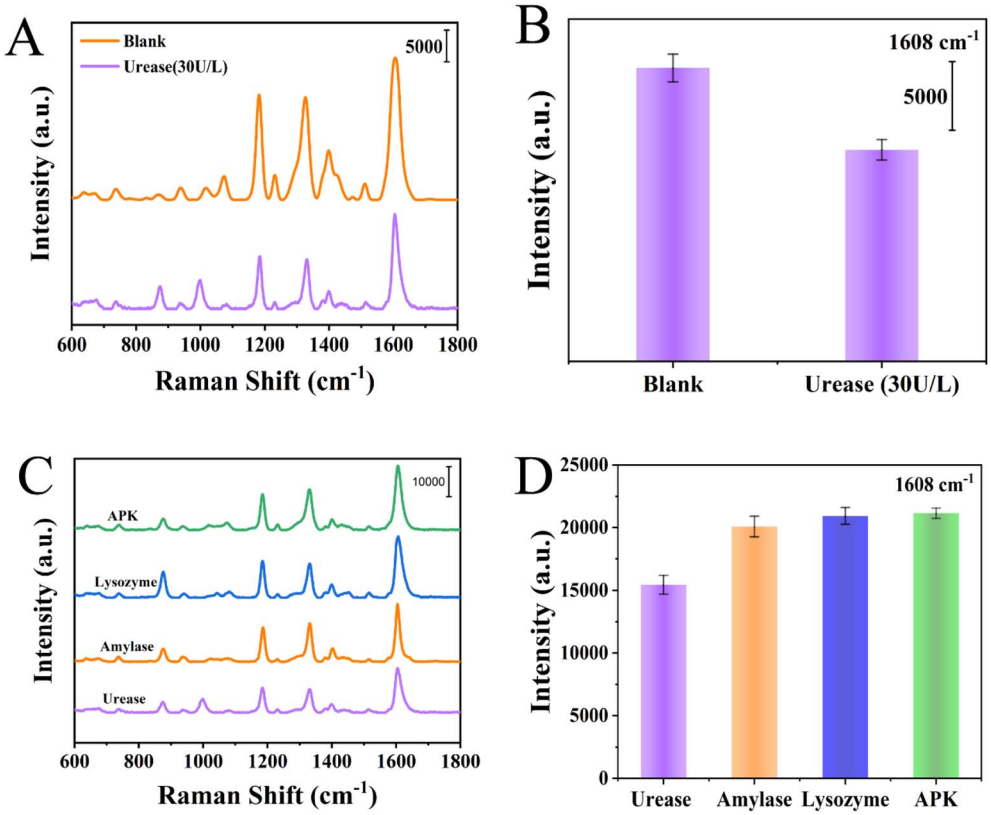

Fig. 4 (A) SERS spectra of a 30 U per L urease solution and blank solution detected by the nano-enzymatic SERS sensor and a blank control group. (B) Histogram of the SERS intensity corresponding to the characteristic peak at 1608 cm^{-1}. (C) SERS spectra corresponding to the addition of urease and different interferents. (D) Histogram of the SERS intensity corresponding to the characteristic peak at 1608 cm^{-1}.

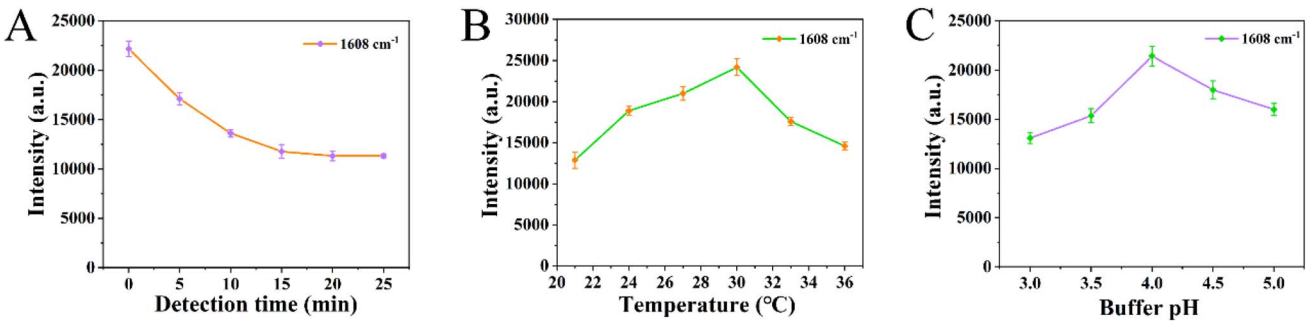

Fig. 5 (A) Line graph of the SERS intensity of the nano-enzymatic SERS sensor at different detection times. (B) Line graph of the SERS intensity of the Au@Pd NRs SERS at different temperatures. (C) Line graph of the SERS intensity of the nano-enzymatic SERS sensor at different buffer pH values.

factor in testing this sensor. To measure the SERS intensity of the mixed solutions under different pH conditions, equal volumes of the solutions to be tested were added to buffers with varying pH values, and capillaries were inserted into the mixed solutions. As shown in Fig. 5(C), the SERS signal intensity increased with increasing pH. The SERS signal of the characteristic peak at 1608 cm^{-1} was the strongest when the pH was 4.0. Subsequent experiments will be conducted at a temperature of 30 °C and a pH of 4.0.[34–36]

3.5 Performance assessment

To enhance the reliability of the detection results, we evaluated the repeatability and homogeneity of the nano-enzymatic SERS sensor. As illustrated in Fig. 6(A), we prepared five different batches of sensors for SERS detection and recorded their spectra. The overall waveforms of the spectra were consistent, with only slight variations in SERS intensities. The intensities of the characteristic peaks at 1608 cm^{-1} (Fig. 6(B)) also

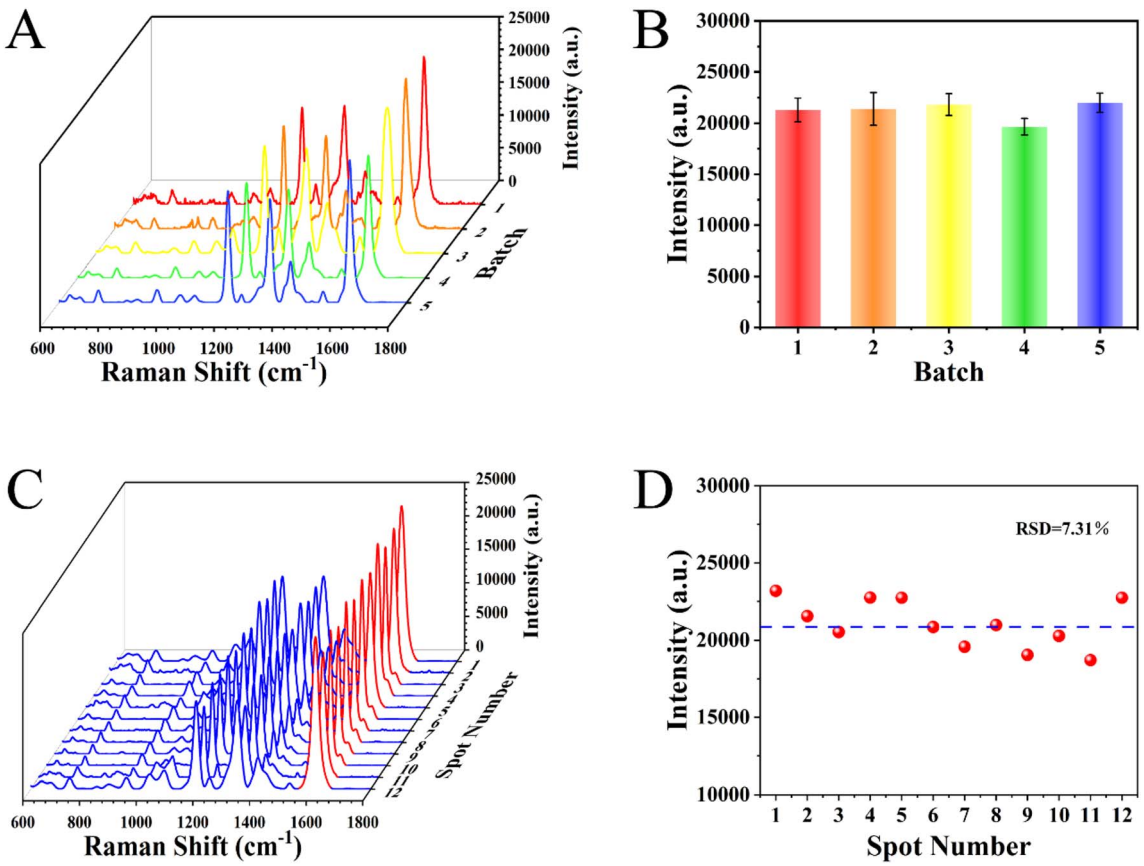

Fig. 6 (A) SERS spectra and (B) histogram of SERS intensity of different batches of nano-enzymatic SERS sensors, with a characteristic peak at 1608 cm^{-1}. (C) SERS spectra and (D) scatter plot of SERS intensity of 12 randomly selected points on the nano-enzymatic SERS sensor, with a characteristic peak at 1608 cm^{-1}.

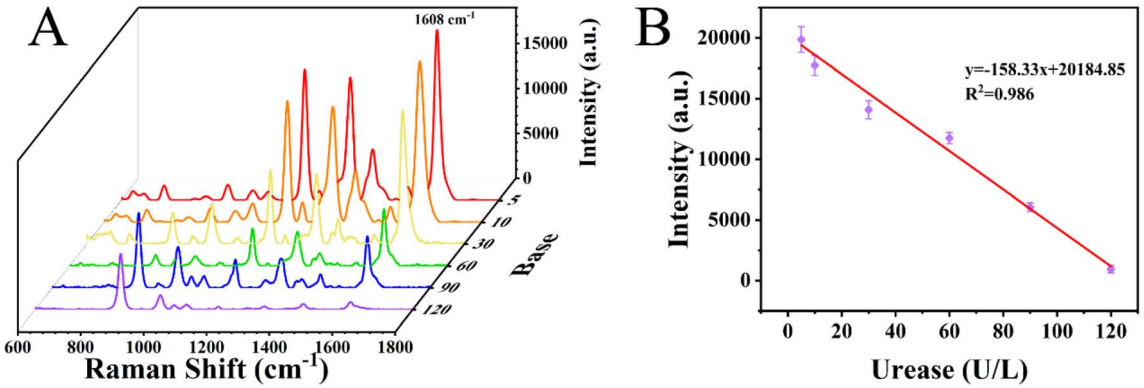

Fig. 7 (A) SERS spectra of the nano-enzymatic SERS sensor for the detection of urease at different concentrations. (B) The calibration curve of the characteristic peak intensity *versus* urease concentration at 1608 cm^{-1}.

Table 1 Comparison of the nano-enzymatic SERS sensors prepared in this paper with existing research methods

Method	LOD	Detection time	Ref.
Immunoassay	0.5 U mL^{-1}	20 min	38
Colorimetry	12.81 mg L^{-1}	4 min	39
Fluorescence	0.002 mg mL^{-1}	35 min	40
SERS	6.09 U L^{-1}	15 min	This work

demonstrated consistency, with a relative standard deviation (RSD) of 6.09%. This indicates that our prepared nano-enzymatic SERS sensors exhibit good signal reproducibility. Then, we randomly selected 12 points on different locations of the sensor surface for SERS detection. The resulting spectra are presented in Fig. 6(C), showing similar spectral patterns with minor differences. The characteristic peak intensity at 1608 cm^{-1} (Fig. 6(D)) had an RSD value of 7.31%, thus confirming the good homogeneity of the sensor structure.

3.6 Quantitative analysis

Under the optimized conditions, the reaction was completed by adding different concentrations of urease to the urea solution. After the addition of buffer, TMB, and H_2O_2, the mixed solutions containing different urease concentrations (5 U L^{-1}, 10 U L^{-1}, 30 U L^{-1}, 60 U L^{-1}, 90 U L^{-1}, and 120 U L^{-1}) were subjected to SERS detection using the nano-enzymatic SERS sensor; the corresponding SERS profiles are shown in Fig. 7(A). This approach was employed to quantitatively characterize the nano-enzymatic SERS sensor. The intensity of the characteristic peak at 1608 cm^{-1} decreased gradually with increasing urease concentration. As shown in Fig. 6(B), a clear linear correlation was observed between the SERS intensity of the characteristic peak at 1608 cm^{-1} and the concentration of urease. The linear equation was $y = -158.33x + 20\,184.85$, with an R^2 value of 0.986. The limit of detection (LOD) was calculated using the equation LOD = i(blank) − 3sd, where i(blank) represents the SERS signal of the blank control, and 3sd is three times the standard deviation.[37] The calculated LOD value was 6.09 U L^{-1}. Compared to other detection strategies previously reported (Table 1), the SERS sensor we developed for nanoenzymes demonstrates significant advantages. This sensor enables sensitive detection of low concentrations of urease.

3.7 Clinical samples analysis

To assess the clinical applicability of the nano-enzymatic SERS sensor, we tested 30 infected and 30 healthy individuals using

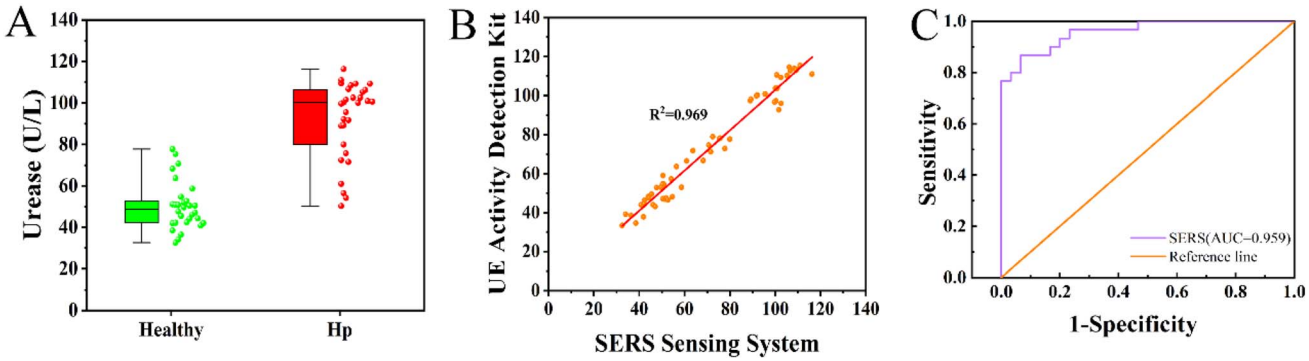

Fig. 8 (A) Half-box line plot of urease concentration in real saliva samples detected by the nano-enzymatic SERS sensor. (B) Correlation study of expression levels of urease in real saliva samples detected by nano-enzymatic SERS sensor and urease activity detection kit. (C) ROC curves to assess the accuracy of the nano-enzymatic SERS sensor assay for diagnosing healthy individuals *versus H. pylori* patients.

Table 2 Comparison of the nano-enzymatic SERS sensor and urease activity detection kit in terms of *H. pylori* detection in clinical samples

Sample	SERS (U L^{-1}) urease	UE activity detection kit (U L^{-1}) urease	Relative error (%) urease
Healthy	50.08	51.36	−2.48
H. pylori	92.31	95.65	−3.49

the sensor to quantify the urease content in their saliva. The collected saliva samples were placed into centrifuge tubes and centrifuged at 9000 rpm for 10 min at 4 °C. Subsequently, the supernatants were collected for SERS detection. The obtained SERS signal intensity was then substituted into the corresponding regression equation (Fig. 7(B)) to determine the urease content in the saliva of the clinical samples (Fig. 8(A)). The average SERS spectra of urease measured in the saliva of healthy and infected individuals are presented in Fig. 7. There was a substantial increase in the amount of urease in infected individuals compared to healthy individuals. The nano-enzymatic SERS sensor proposed in this study exhibited a significant correlation (Table S1 and S2), with a correlation coefficient of 0.969, when compared with the results obtained using the urease detection kit (Fig. 8(B)) (Table 2). A receiver operating characteristic (ROC) curve was introduced to evaluate the diagnostic efficacy of the sensor (Table S3). Based on the analysis of the area under the ROC curve (AUC), the Au@Pd NRs SERS demonstrated a good classification effect (Fig. 8(C)). The results indicate that the Au@Pd NRs SERS developed in this study shows high accuracy and excellent diagnostic efficacy in clinical testing, and it has very broad application prospects.

4. Conclusions

In this study, a pH-responsive nano-enzymatic SERS sensor was successfully developed, which enables the rapid, simple, and sensitive diagnosis of *H. pylori*. The nano-enzymatic SERS sensor with SERS activity and POD-like activity was obtained by assembling the nano-enzymatic Au@Pd NRs on the inner wall of the capillary. It exhibited excellent detection performance, including specificity, homogeneity, reproducibility, and detection range. The assay can be accomplished in less than 15 min, the LOD was as low as 6.09 U L^{-1}, and the linear range was 5–120 U L^{-1}, realizing the rapid and sensitive detection of urease concentration. The correlation coefficient between the nano-enzymatic SERS sensor and the urease detection kit for detecting urease concentration in clinical saliva samples was analyzed, and the correlation coefficient was 0.969, which indicated that the detection results had a high accuracy. A receiver operating characteristic (ROC) curve was introduced to assess the diagnostic efficacy of the sensor for the detection of *H. pylori*, and the analysis showed an AUC value of 0.959, indicating that the nano-enzymatic SERS sensor has a good classification effect. In conclusion, this pH-responsive nano-enzymatic SERS sensor has good application prospects in clinical diagnosis and proposes a new method for POCT of *H. pylori*.

Conflicts of interest

There are no conflicts to declare.

Data availability

All data supporting this study are included in the article and its SI. Supplementary information is available. See DOI: **https://doi.org/10.1039/d5ra05046d**.

Acknowledgements

This work was supported by the National Natural Science Foundation of China (project code: 81403232), the Major Programs of Natural Science Foundation of Higher Education in Jiangsu Province (19KJA480003), and the Natural Science Foundation of Jiangsu Province (No. BK20171290).

References

1 B. Liang, Y. Yuan, X.-J. Peng, X.-L. Liu, X.-K. Hu and D.-M. Xing, *Front. Cell. Infect. Microbiol.*, 2022, **12**, 1042070.
2 K. O. Alfarouk, A. H. H. Bashir, A. N. Aljarbou, A. M. Ramadan, A. K. Muddathir, S. T. S. AlHoufie, A. Hifny, G. O. Elhassan, M. E. Ibrahim, S. S. Alqahtani, S. D. AlSharari, C. T. Supuran, C. Rauch, R. A. Cardone, S. J. Reshkin, S. Fais and S. Harguindey, *Front. Oncol.*, 2019, **9**, 75.
3 M. P. Dore, G. M. Pes, G. Bassotti and P. Usai-Satta, *Gastroenterol. Res. Pract.*, 2016, **2016**, 8463614.
4 X. Wang, D. Zhu, S. Li, Y. Dai, G. Teng and W. Wang, *Dig. Dis. Sci.*, 2024, **69**, 1293–1301.
5 W. You, L. Zhang, K. Pan and J. Ma, *Prog. Chem.*, 2013, **25**, 1575–1582.
6 H. Suzuki and H. Mori, *Gan to Kagaku Ryoho*, 2018, **45**, 1123–1127.
7 J.-H. Kim, *Korean J. Helicobacter Up. Gastrointest. Res.*, 2014, **14**, 233–236.
8 D. S. Bordin, I. N. Voynovan, S. Kolbasnikov and Y. Embutnieks, *Ter. Arkh.*, 2018, **90**, 133–139.
9 A. B. M. Carlos, C. V. de Oliveira, M. A. M. Rodrigues and V. E. Costa, *Anal. Bioanal. Chem.*, 2019, **411**, 5641–5645.
10 P. Sabbagh, M. Mohammadnia-Afrouzi, M. Javanian, A. Babazadeh, V. Koppolu, V. R. Vasigala, H. R. Nouri and S. Ebrahimpour, *Eur. J. Clin. Microbiol. Infect. Dis.*, 2019, **38**, 55–66.
11 H. Shaalan, M. Azrad and A. Peretz, *Front. Microbiol.*, 2024, **15**, 1464484.
12 O. Guzel-Akdemir and A. Akdemir, *Expert Opin. Ther. Pat.*, 2025, **35**, 17–30.
13 H. Fan, K. I. Wong, Y. Ma, M. Li, H. Li, L. Wei, S. Wang, M. Yao and M. Lu, *Adv. Funct. Mater.*, 2025, 35–36.
14 Y. Mi, Y. Yan, M. Wang, L. Yang, J. He and Y. Jiang, *Nanophotonics*, 2022, **11**, 559–570.
15 Q.-F. He, Y.-J. Zhang, Z.-L. Yang, J.-C. Dong, X.-M. Lin and J.-F. Li, *Chin. J. Chem.*, 2023, **41**, 355–369.

16 J. Guo, F. Zeng, J. Guo and X. Ma, *J. Mater. Sci. Technol.*, 2020, **37**, 96–103.
17 L. A. Jakob, W. M. Deacon, Y. Zhang, *et al.*, *Nat. Commun.*, 2023, **14**, 3291.
18 R. Chen, S. Li, S. Ren, D. Han, K. Qin, X. Jia, H. Zhou and Z. Gao, *Adv. Colloid Interface Sci.*, 2024, **331**, 103235.
19 Q. Yang, J. Wang, H. Wu, S. Qin, J. Pan and C. Li, *Appl. Surf. Sci.*, 2022, **598**, 153746.
20 S. Ding, L. He, X. Bian and G. Tian, *Nano Today*, 2020, **35**, 100920.
21 L. Zhang, Q. Dong and Y. Hao, *Adv. Sci.*, 2023, **10**(30), e2302703.
22 X.-M. Xia, X. Zhang, Y.-J. Wend, L. Zhang and R.-Y. Tang, *Chin. J. Inorg. Chem.*, 2021, **37**, 809–816.
23 G. Fu, S. T. Sanjay, W. Zhou, *et al.*, *Anal. Chem.*, 2018, **90**(9), 5930–5937.
24 K. Kumar, M. M. Shafeeq, P. Kumar, R. Munjal, S. Mukhopadhyay, D. P. Mondal, M. A. Khan and V. Vandana, *Microchim. Acta*, 2024, **191**, 357.
25 H. K. Nguyen, A. T. Dao, T. T. Tran, H. L. Nguyen, H. T. Nguyen and V. T. H. Le, *Plasmonics*, 2021, **16**, 2125–2137.
26 C. H. Lee, L. Tian and S. Singamaneni, *ACS Appl. Mater. Interfaces*, 2010, **2**, 3429–3435.
27 N. R. Barveen, T.-J. Wang and Y.-H. Chang, *Microchem. J.*, 2020, **159**, 105520.
28 L. Lv, L. He, S. Jiang, J. Chen, C. Zhou, J. Qu, Y. Lu, P. Hong, S. Sun and C. Li, *Sci. Total Environ.*, 2020, **728**, 138449.
29 J. W. Lee, K. Kim and K. S. Shin, *Vib. Spectrosc.*, 2010, **53**, 121–125.
30 B. V. Zhmud, F. Tiberg and K. Hallstensson, *J. Colloid Interface Sci.*, 2000, **228**, 263–269.
31 S. Yueksel, A. M. Schwenke, G. Soliveri, S. Ardizzone, K. Weber, D. Cialla-May, S. Hoeppener, U. S. Schubert and J. Popp, *Anal. Chim. Acta*, 2016, **939**, 93–100.
32 X. Ye, Y. Gao, J. Chen, D. C. Reifsnyder, C. Zheng and C. B. Murray, *Nano Lett.*, 2013, **13**, 2163–2171.
33 Y. Panahi, R. Yekta, G. Dehghan, S. Rashtbari, B. Baradaran, N. J. Jafari and A. A. Moosavi-Movahedi, *Int. J. Biol. Macromol.*, 2019, **122**, 306–311.
34 B. Liu, Y. Xue, Z. Gao, K. Tang, G. Wang, Z. Chen and X. Zuo, *Colloids Surf., B*, 2021, **208**, 112060.
35 T. Wen, W. He, Y. Chong, Y. Liu, J.-J. Yin and X. Wu, *Phys. Chem. Chem. Phys.*, 2015, **17**, 24937–24943.
36 Z. Khan, *Int. J. Biol. Macromol.*, 2020, **153**, 545–560.
37 J. Xia, Y. Li, Y. Xin, L. Kang and D. Lu, *Microchem. J.*, 2024, **207**, 111750.
38 Z.-X. Wang and S.-N. Ding, *Analyst*, 2023, **148**, 683–689.
39 Y. Wan, Z. Xie, M. Cao, C. Zhang, Z. Feng, B. Tian and Z. Liu, *Microchim. Acta*, 2024, **191**, 679.
40 J. An, Y. Hu, D. Yang, Y. Han, J. Zhang and Y. Liu, *Spectrochim. Acta, Part A*, 2022, **269**, 120705.